Formation of nonbonding π electronic states of graphite due to Pt-C hybridization

Takahiro Kondo,[1] Yosuke Iwasaki,[1] Yujiro Honma,[1] Yoshiteru Takagi,[1,2,3] Susumu Okada,[1,2,3] and Junji Nakamura[1,*]
[1]*Graduate School of Pure and Applied Sciences, University of Tsukuba, 1-1-1 Tennodai, Tsukuba, Ibaraki 305-8573, Japan*
[2]*Center for Computational Sciences, University of Tsukuba, 1-1-1 Tennodai, Tsukuba, Ibaraki 305-8573, Japan*
[3]*CREST, Japan Science and Technology Agency, 4-1-8 Honcho, Kawaguchi, Saitama 332-0012, Japan*
(Received 17 November 2009; published 28 December 2009)

The electronic states of the graphite surface with platinum clusters have been investigated at the atomic scale by scanning tunneling spectroscopy. The distinct local density of states were observed near the Fermi level for carbon atoms around the Pt clusters, which has been ascribed as nonbonding π electronic states of graphite due to Pt-C hybridization. This is consistent with the experimentally observed weaker phonon energies of graphite near the Pt cluster as well as the results of first-principles density-functional calculations of a graphene sheet with a Pt cluster.

DOI: 10.1103/PhysRevB.80.233408 PACS number(s): 73.20.At, 73.20.Hb

The nonbonding π electronic states of graphite-related material such as carbon nanotubes, graphene sheets, and graphite are of special interest to both physics and chemistry because they are the key electronic states to control the electronic devices[1] and maybe the active sites for the specific chemical reactions,[2] respectively. The states are formed near the zig-zag edge of the graphite as "edge state" which was theoretically predicted at first[3] and then experimentally observed by the measurements with scanning tunneling microscope (STM).[4,5] Recent theoretical calculations predict that the states can also appear around the hydrogen atoms bonded with the carbon atom or the defects of graphene sheets.[6] In this Brief Report, we present an experimental observation of the formation of the nonbonding π electronic states due to the adatom-carbon interaction of graphite. We deposited Pt clusters on a highly oriented pyrolytic graphite (HOPG) surface under ultrahigh vacuum (UHV) condition and then investigated its electronic structure at the atomic scale by low-temperature STM. The origin of the observed states has been ascribed to the Pt-C hybridization based on the measurements of STM images, scanning tunneling spectroscopy (STS), inelastic electron-tunneling spectroscopy (IETS), and first-principles density-functional calculations.

All experiments were performed in an UHV STM chamber (UNISOKU, USM-1500) with a base pressure of 2×10^{-10} Torr. HOPG (ZYA grade) was cleaved in air using adhesive tape. Platinum atoms were deposited on HOPG at room temperature by resistive heating of a Pt wire. After the Pt deposition, the sample was cooled to ~6 K with liquid helium. The surface morphology, the surface electronic structure, and the surface vibrational properties were then examined by STM, STS, and IETS with a PtIr tip. STM images were recorded in constant-current mode (current image) and constant-height mode (height image).

A typical STM current image of the Pt-deposited HOPG is shown in Fig. 1(a). The Pt atoms are seen on a terrace of graphite as bright spots in the STM image. The Pt atoms form flat clusters 1–2 atoms in height and 2–5 nm wide as shown by the height-width distribution in Fig. 1(b). This indicates the Pt-C interactions are stronger than the Pt-Pt interactions. The height-width distribution is similar to Pt nanoclusters which have been reported previously.[7]

The atomic scale STM images are shown in Figs. 1(c) and 1(d). The HOPG substrate displays bright spot arrays with a periodicity of 0.246 nm. These bright spots correspond to the so-called β carbon, i.e., the carbon atoms located above the centers of the hexagons of the layer beneath; the remaining carbon atoms are α-carbon atoms.[8] In the vicinity of a Pt cluster, clear modulation of the electronic state of the substrate graphite was observed as superstructures as shown in Fig. 1(c) and as previously reported.[9,10] The tunneling current related to the superstructure gradually increases as the tip approaches the Pt cluster, as shown by the arrows in the line profile of Fig. 1(e), suggesting that the modulation of the electronic states propagates from the Pt cluster. Two types of superstructures can be seen; the $(\sqrt{3}\times\sqrt{3})R30°$ structure and the honeycomb structure. These superstructures have also been reported on graphite surfaces around other metal clusters,[11,12] defects,[13–19] and edges.[5,20–22] The appearance of the $(\sqrt{3}\times\sqrt{3})R30°$ structure has been interpreted as the modulation of the periodic charge density and/or interference between normal and scattered electron wave functions, such as standing waves, by adatoms, defects, or edges,[5,11–25] while the honeycomb structure has been attributed to the superposition of two $(\sqrt{3}\times\sqrt{3})R30°$ structures propagating from two different defects and/or edges of the graphite.[5,18] As shown in Fig. 1(d), these superstructures do not always appear at the relatively high bias voltages as reported previously,[15] supporting the above interpretations that the superstructures are not the real atom arrangement but are the result of the modulation of the electronic structure of the surface.

To elucidate the adsorption site and characteristics of a typical Pt cluster on graphite, the line profile of the height image Fig. 1(d) has been plotted in Fig. 1(f). The Pt cluster consists of monoatomic heights with a similar periodicity and amplitude to the bright spots on the substrate. The corrugation measured over the Pt cluster in Fig. 4(f) is due to corrugation in the positions of the Pt ion cores; if it were a transmission of the underlying graphite corrugation, the amplitude of corrugation would be lower on top of the Pt island than on top of graphite. These results suggest the Pt monolayer clusters on HOPG exhibit three characteristics: (i) the electronic structure is spatially localized because of the stepwise height difference in the STM line profile, (ii) Pt atoms are located over the β-carbon sites to form a commensurate

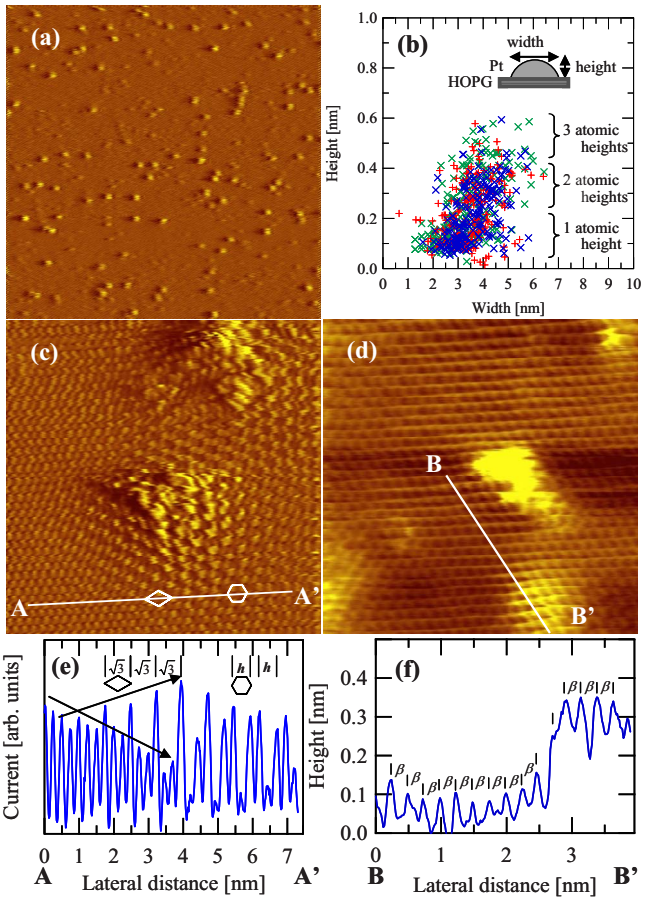

FIG. 1. (Color online) (a) STM current image of the Pt-deposited HOPG at 17 K (129×129 nm^2, sample bias $V_s=-101$ mV, tunneling current $I_t=157$ pA). (b) Height-width distribution of the Pt clusters estimated from three different height images (129×129 nm^2) containing 586 Pt clusters that have been obtained at respective three different sample positions. The different colors represent the differences in the analyzed images. Both height and size do not show distinct values due to the resolution limit of the clusters in the large size images. The exact height and size values are obtained from high-resolution height images such as (d). (c) STM current image at 6.1 K (8.4×8.4 nm^2, $V_s=249$ mV, $I_t=205$ pA). (d) STM height image at 6.1 K (6.3×6.3 nm^2, $V_s=308$ mV, $I_t=201$ pA). (e) Line profile along AA' in the STM current image c, where $\sqrt{3}$ and h represent the $(\sqrt{3}\times\sqrt{3})R30°$ structure and the honeycomb structure, respectively. (f) Line profile along BB' line in the STM height image d, where β represents the peak position difference of 0.246 nm.

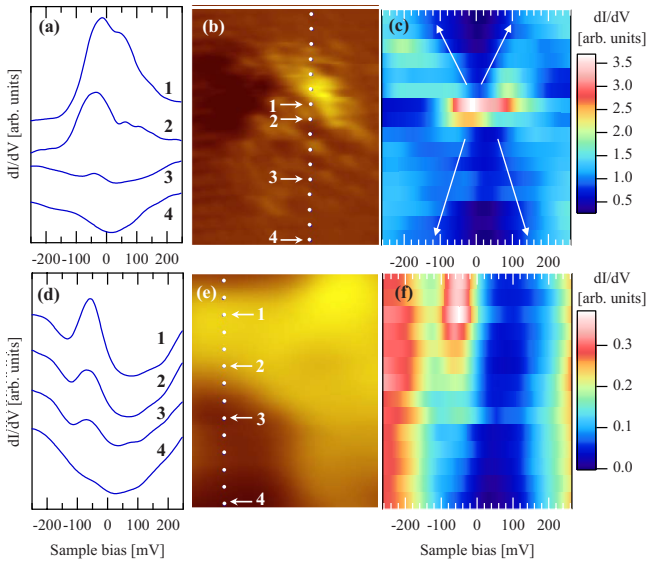

FIG. 2. (Color online) (a) STS spectra of the Pt-deposited HOPG at 5.8 K (see text). (b) STM height image obtained during STS measurement (3.1×3.9 nm^2, $V_s=305$ mV, $I_t=117$ pA). (c) Space-resolved STS spectra. (d)–(f) are the same series of the measurements as (a)–(c) obtained around a different Pt cluster on HOPG at 6.5 K (0.6×0.5 nm^2, $V_s=303$ mV, $I_t=132$ pA). In all cases, ten STS spectra were measured and the averaged spectra are shown.

monolayer structure possibly as a result of the stronger Pt-C interaction, and (iii) the Pt-Pt distance, 0.246 nm, is considerably less than the shortest Pt-Pt distance of 0.277 nm in the single crystalline Pt—a reduction of 13%. The reduction should induce a modification in the electronic structure of the nanocluster on graphite. These characteristics agree with the results in the literatures.[7,9,25–28]

STS spectra taken near the Pt cluster are shown in Fig. 2(a). The spectrum was measured at locations 1–4 in a STM image, shown in Fig. 2(b). The brighter spots in Fig. 2(b) (such as position 1) correspond to Pt atoms with monoatomic height, while the other spots correspond to C atoms (such as positions 2, 3, and 4). Figure 2(c) shows the spatially resolved STS spectra obtained across the Pt cluster with the vertical axis being taken from along the white dots in Fig. 2(b). The same measurements conducted around a different Pt cluster with a smaller scan area are shown in Figs. 2(d)–2(f). Figures 2(a) and 2(d) show that a distinct peak near the Fermi level appears on the Pt atoms and on the carbon atoms in the vicinity of the Pt cluster. Such a peak frequently appears in the $0\sim-80$ meV range in the vicinity of the Pt clusters, indicating that a new local density of states appears at the occupied state around the Pt cluster.

There are three possible assignments of the new electronic states observed in Fig. 2. They could be (i) states solely associated with the Pt cluster, (ii) states arising from the quantum size effect of metal nanoclusters,[29] or (iii) states associated with the carbon atoms due to the interaction between the Pt clusters and the graphite. The third explanation is the most plausible with the distinct STS peak near the Fermi level being a nonbonding π electronic state of graphite due to Pt-C hybridization, which is similar to the edge state of a graphite ribbon.[3] The assignment is based on the following facts: (1) The distinct STS peak can be observed on the carbon atoms in the vicinity of the Pt cluster as well as on the Pt atom as shown in Figs. 2(a) and 2(d). (2) The intensity of this STS peak decreases with increasing distance from the Pt cluster as shown in Figs. 2(a) and 2(d). Following the arrows in Fig. 2(c), it is clear that the spectrum ($-200\sim200$ meV) does not change in a stepwise manner, but peak intensity gradually weakens with increasing distance from Pt cluster, suggesting the new electronic states propagate into the area around the Pt cluster. For the carbon atoms far from the Pt cluster, a parabolic shape is obtained in the STS spectrum

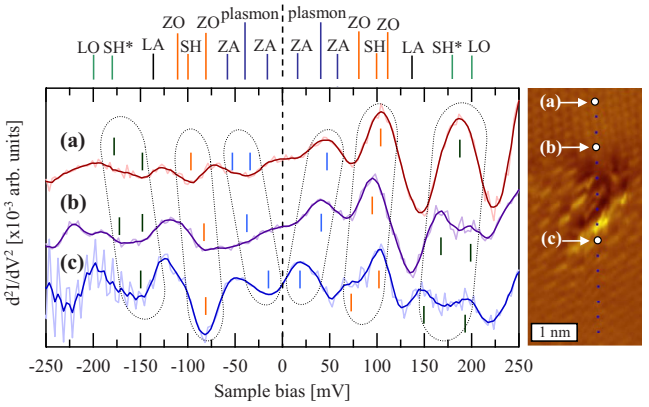

FIG. 3. (Color online) IETS spectra at 5.8 K obtained on the carbon atoms far from the Pt cluster (a), in the vicinity of the Pt cluster (b), and adjacent to the Pt cluster as indicated by the arrows in the STM height image (V_s=291 mV, I_t=143 pA). For comparison, the vibrational modes and plasmon peak energies (Ref. 32) are marked at the top of the figure. The phonon branches are specified as follows: out-of-plane acoustic (ZA), acoustic shear (SH), longitudinal acoustic (LA), out-of-plane optical (ZO), optical shear (SH*), and longitudinal optical (LO).

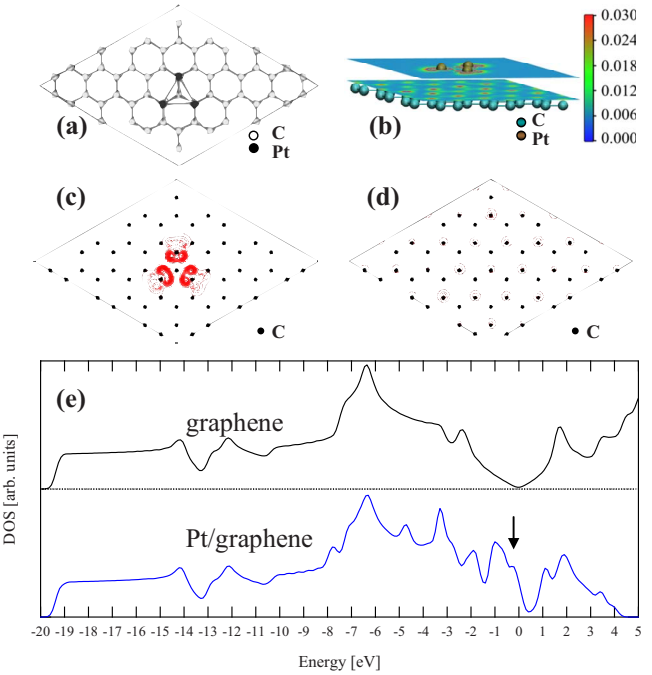

FIG. 4. (Color online) (a) The schematic model of the calculated graphene sheet with a Pt cluster. (b) Calculated spatial distribution of the integrated local density of state from E_f to −0.2 eV at different heights [the distribution above 0.053 nm and 0.233 nm are shown with red circles in (c) and (d)]. (e) Calculated total density of state of graphene and Pt/graphene, where the spectra are normalized by the each of the peak intensity for easy comparison. The Fermi energy for Pt/graphene has been shifted to −0.1 eV to obtain the same energy level at the bottom of the s band between the results for graphene and for Pt/graphene.

corresponding to the tails of the π and π^* states of graphite. (3) Pt atoms are known to have no distinct energy levels in the range investigated here.[30,31]

The formation of the nonbonding π electronic states is proposed here to be due to the Pt-C hybridization between filled or empty Pt 5d orbitals and π or π^* graphite states of the β-carbon atoms. As a result of the hybridization between Pt atoms and β-carbon atoms, the nonbonding π electronic states appear on the surrounding α-carbon atoms due to the rehybridizing of the conjugated bonds between α-carbon and β-carbon atoms. This would involve the two p_z orbitals, previously forming the bond between α- and β-carbon atoms. The p_z orbital of β carbon would now be hybridized with a d orbital of the Pt atom and p_z orbital of α carbon becomes a nonbonding π orbital. The electrons of the conjugated bond probably move to the nonbonding orbital which leads to the appearance of the new state at the occupied state at the vicinity of the Pt cluster. Note that the nonbonding state was observed on carbon atoms up to sub-nm distances from Pt atoms. That is, the intensity of the STS peak attenuated gradually with increasing distance from Pt atom. In this model, the nonbonding state of the α carbon thus spreads out in two dimensions.

The proposed model explains the IETS results as well as the STS results. Figures 3(a)–3(c) show the IETS spectra measured on the carbon atoms far from, in the vicinity of, and adjacent to the Pt atom, respectively, as indicated by the arrows in the STM height image in Fig. 3. The reported phonon and plasmon energies from the literature[32] are marked at the top of the figure for comparison. The symmetrical peaks, which appear at positive and negative sample biases in Fig. 3, are found to shift toward a zero sample bias with decreasing distance from Pt atom [Figs. 3(a)–3(c)] as shown by the shaded shapes. The shift implies a smaller phonon energy in the graphite, suggesting the C-C bonds have weaker binding energies. This weakening is ascribed to the rehybridization of the conjugated bond around the Pt cluster as a result of Pt-C hybridization.

To confirm the above model, a graphene sheet with a Pt cluster has been studied by using the generalized gradient approximation (GGA) with the Perdew-Burke-Ernzerhof functional[33] in the framework of density-functional theory (DFT) calculations. The ultrasoft pseudopotentials are adopted for describing the electron-ion interaction.[34] The valence wave function has been expanded in terms of the plane-wave basis set with cutoff energy of 36 Ryd. The calculations were made using the Tokyo *Ab initio* Program Package (TAPP).[35] The schematic model of the graphene sheet with the Pt cluster as calculated is shown in Fig. 4(a). Three Pt atoms are located on top of carbon atoms to reproduce our experimentally observed adsorption structure from Fig. 1(d). The structure of the Pt cluster has been optimized to below 0.002 h/a.u. This has resulted in a stable, shorter Pt-Pt distance of 0.257 nm on graphite, which qualitatively agrees with the experimentally observed Pt structure. Slices through the calculated spatial distribution of the integrated local density of state from E_f to −0.2 eV are shown in Figs. 4(b)–4(d). Figure 4(e) shows the calculated total density of states of both graphene and the Pt cluster on graphene. The peaks which appear near the Fermi level in the Pt/graphene case are indicated with an arrow. It is clear that the new state

near the Fermi level appears on the carbon atoms adjacent to the Pt atom. The state propagates out from the Pt clusters as shown in Fig. 4(d). These results agree with experimentally observed STS spectra shown in Fig. 2, suggesting that the calculation reproduces the experimentally observed features, even though the calculation does not take into account the underlying graphene layers in the graphite due to the difficulties in the including the interactions of the graphene layers, such as van der Waals force, in the calculation.

In summary, distinct STS peaks were found near the Fermi level at the carbon atoms around the Pt clusters. The peak has been assigned as nonbonding π electronic states of the graphite and the origin of these states formation has been ascribed to Pt-C hybridization based on the measurements of STM, STS, and IETS, and DFT calculations.

We appreciate financial support from NEDO (New Energy and Industrial Technology Development).

*Corresponding author; nakamura@ims.tsukuba.ac.jp

[1] A. H. Castro Neto *et al.*, Rev. Mod. Phys. **81**, 109 (2009); K. A. Ritter, Nature Mater. **8**, 235 (2009); D. A. Areshkin, Nano Lett. **7**, 204 (2007); Y. Yoon and G. Jing, Appl. Phys. Lett. **91**, 073103 (2007); D. Basu *et al.*, *ibid.* **92**, 042114 (2008).
[2] K. Takahara *et al.*, Phys. Rev. B **76**, 035442 (2007); D. Jiang *et al.*, J. Phys. Chem. **126**, 134701 (2007).
[3] K. Kobayashi, Phys. Rev. B **48**, 1757 (1993); D. J. Klein, Chem. Phys. Lett. **217**, 261 (1994); M. Fujita *et al.*, J. Phys. Soc. Jpn. **65**, 1920 (1996).
[4] Z. Klusek *et al.*, Appl. Surf. Sci. **161**, 508 (2000).
[5] Y. Kobayashi *et al.*, Phys. Rev. B **71**, 193406 (2005); Y. Niimi *et al.*, *ibid.* **73**, 085421 (2006).
[6] T. O. Wehling *et al.*, Chem. Phys. Lett. **476**, 125 (2009); X. Yang *et al.*, Carbon **47**, 1399 (2009); S. Casolo *et al.*, J. Chem. Phys. **130**, 054704 (2009).
[7] T. Kondo *et al.*, J. Phys. Chem. C **112**, 15607 (2008).
[8] D. Tománek *et al.*, Phys. Rev. B **35**, 7790 (1987).
[9] F. Atamny and A. Baiker, Appl. Catal., A **173**, 201 (1998).
[10] J. Xhie *et al.*, Phys. Rev. B **43**, 8917 (1991); J. Vac. Sci. Technol. B **9**, 833 (1991).
[11] H. Xu *et al.*, Surf. Sci. **325**, 285 (1995).
[12] M. Kuwahara *et al.*, Surf. Sci. **344**, L1259 (1995).
[13] H. A. Mizes, Science **244**, 559 (1989).
[14] K. F. Kelly and N. J. Halas, Surf. Sci. **416**, L1085 (1998).
[15] J. G. Kushmerick *et al.*, J. Phys. Chem. B **103**, 1619 (1999).
[16] P. Ruffieux *et al.*, Phys. Rev. B **71**, 153403 (2005).
[17] Y. Ferro and A. Allouche, Phys. Rev. B **75**, 155438 (2007).
[18] J. C. Moreno López *et al.*, Surf. Sci. **602**, 671 (2008).
[19] L. Tapasztó *et al.*, Physica E **40**, 2263 (2008).
[20] P. L. Giunta and S. P. Kelty, J. Chem. Phys. **114**, 1807 (2001).
[21] Y. Niimi *et al.*, Appl. Surf. Sci. **241**, 43 (2005).
[22] W. Pong and C. Durkan, J. Phys. D **38**, R329 (2005).
[23] G. M. Shedd and P. E. Russell, Surf. Sci. **266**, 259 (1992).
[24] J. Valenzuela-Benavides and L. M. de la Garza, Surf. Sci. **330**, 227 (1995).
[25] K. Sattler, Z. Phys. D:At., Mol. Clusters **19**, 287 (1991).
[26] G. W. Clark and L. L. Kesmodel, J. Vac. Sci. Technol. B **11**, 131 (1993).
[27] S. Eppell *et al.*, Langmuir **6**, 1316 (1990).
[28] U. Muller *et al.*, J. Vac. Sci. Technol. B **9**, 829 (1991).
[29] A. Bettac *et al.*, Surf. Sci. **402**, 475 (1998); H. Hovel *et al.*, *ibid.* **463**, L603 (2000).
[30] W. Eberhardt *et al.*, Phys. Rev. Lett. **64**, 780 (1990).
[31] W. Di *et al.*, Phys. Rev. B **45**, 3652 (1992); **43**, 12062 (1991).
[32] L. Vitali *et al.*, Phys. Rev. B **69**, 121414 (2004).
[33] J. P. Perdew *et al.*, Phys. Rev. Lett. **77**, 3865 (1996).
[34] D. Vanderbilt, Phys. Rev. B **41**, 7892 (1990).
[35] M. Tsukada *et al.*, Computer program package TAPP, University of Tokyo, Tokyo, Japan, 1983–2009.